9-2-2021

# An Examination of Factors Influencing Small Proton Chemical Shift Differences in Nitrogen-Substituted Monodeuterated Methyl Groups

Stuart J. Elliott

O. Maduka Ogba

Lynda J. Brown

Daniel J. O'Leary

# An Examination of Factors Influencing Small Proton Chemical Shift Differences in Nitrogen-Substituted Monodeuterated Methyl Groups

symmetry

MDPI

*Article*

# An Examination of Factors Influencing Small Proton Chemical Shift Differences in Nitrogen-Substituted Monodeuterated Methyl Groups

**Stuart J. Elliott [1,*], O. Maduka Ogba [2], Lynda J. Brown [3] and Daniel J. O'Leary [4,*]**

[1] Department of Chemistry, University of Liverpool, Liverpool L69 7ZD, UK
[2] Chemistry and Biochemistry Program, Schmid College of Science and Technology, Chapman University, Orange, CA 92886, USA; ogba@chapman.edu
[3] School of Chemistry, University of Southampton, Southampton SO17 1BJ, UK; L.J.Brown@soton.ac.uk
[4] Department of Chemistry, Pomona College, Claremont, CA 91711, USA
* Correspondence: Stuart.Elliott@liverpool.ac.uk (S.J.E.); Daniel.O'Leary@pomona.edu (D.J.O.)

**Abstract:** Monodeuterated methyl groups have previously been demonstrated to provide access to long-lived nuclear spin states. This is possible when the $CH_2D$ rotamers have sufficiently different populations and the local environment is chiral, which foments a non-negligible isotropic chemical shift difference between the two $CH_2D$ protons. In this article, the focus is on the *N*-$CH_2D$ group of *N*-$CH_2D$-2-methylpiperidine and other suitable $CH_2D$-piperidine derivatives. We used a combined experimental and computational approach to investigate how rotameric symmetry breaking leads to a $^1H$ $CH_2D$ chemical shift difference that can subsequently be tuned by a variety of factors such as temperature, acidity and 2-substituted molecular groups.

**Keywords:** monodeuterated methyl group; $CH_2D$; chemical shift difference; equilibrium isotope effects; diastereotopicity



**Citation:** Elliott, S.J.; Ogba, O.M.; Brown, L.J.; O'Leary, D.J. An Examination of Factors Influencing Small Proton Chemical Shift Differences in Nitrogen-Substituted Monodeuterated Methyl Groups. *Symmetry* **2021**, *13*, 1610. https://doi.org/10.3390/sym13091610

Academic Editor: Gabriele Stevanato

Received: 29 July 2021
Accepted: 26 August 2021
Published: 2 September 2021



## 1. Introduction

The decay of conventional magnetization in the majority of traditional solution-state nuclear magnetic resonance (NMR) experiments is limited by the longitudinal relaxation time constant $T_1$. Long-lived states (LLS) are magnetically silent, sheltered from NMR relaxation and decay with extended lifetimes [1–4], providing an opportunity to alleviate this limitation. For nuclear spin-1/2 pairs, the LLS is defined as the mean population imbalance between the exchange-antisymmetric nuclear singlet state and the exchange-symmetric nuclear triplet states. The long-lived property is known as nuclear singlet order and has the corresponding relaxation time constant denoted $T_S$, which often surpasses $T_1$ by a large factor [5–9]. LLS have applications to spatial NMR imaging with strongly improved contrast originating from differences in LLS lifetimes [10], ligand-binding with enhanced contrast between free and bound ligands which requires a protein–ligand ratio ca. 25 times lower than traditional NMR methods [11] and reaction monitoring of the enzymatic conversion of fumarate to malate [12]. The combination of LLS with hyperpolarization techniques has shown promising results [13–16].

Access to singlet order is provided via a break in the symmetry of the coherent nuclear spin Hamiltonian, which can be induced by a chemical shift difference between the constituents of the nuclear spin-1/2 pair [17–19]. Small chemical shift differences in nuclear spin-1/2 pairs have previously been achieved by: (*i*) Synthetic design. Hill-Cousins et al. synthesized a $^{13}C_2$-labelled derivative of naphthalene with a small chemical shift difference between the $^{13}C$ nuclear sites by introducing specifically tailored molecular groups on either side of the two naphthalene rings [20]. This molecule supports an LLS with a lifetime which exceeds 1 h in room-temperature solution [21]; (*ii*) Isotopic substitution. Tayler and Levitt incorporated $^{18}O$ isotopic labelling to engender a small $^{13}C$ chemical shift difference

in a symmetric oxalate molecule [22]; (*iii*) Altering pH. Pravdivtsev et al. adjusted the pH of their solution to tailor the chemical shift difference between the $CH_2$ group protons of *N*-acetyl-L-aspartic acid [23]; and (*iv*) Chemical reactions. Zhang et al. forged a symmetry-breaking $^1H$ chemical shift difference and unlocked access to the LLS of dimethyl maleate by the addition of thiols [24].

In this article, we employ a blend of experimental and computational methods to assess the symmetry-breaking requirements to forge an appreciable chemical shift difference between the $CH_2D$ protons in the monodeuterated methyl group of *N*-$CH_2D$-2-methylpiperidine, which allows access to the $CH_2D$ LLS. We further tailor the magnitude of the $CH_2D$ proton chemical shift difference by several environmental influences such as temperature, acidity and nearby molecular groups.

## 2. *N*-$CH_2D$-2-methylpiperidine

### *2.1. Symmetry Breaking*

For a monodeuterated methyl ($CH_2D$) group in a chiral molecule, the two $CH_2D$ protons are diastereotopic and can have distinct chemical shifts. An observable $CH_2D$ proton chemical shift difference is much more difficult to achieve, however, and chemical inequivalence of $CH_2D$ protons has only been reported in a few select molecules, the majority of which incorporate an *N*-$CH_2D$ group in a chiral setting [25–31].

An observable diastereotopic chemical shift difference between the two protons of a $CH_2D$ group is most readily forged by combining two important factors [32]:

1. A considerable rotameric preference/aversion for a particular $CH_2D$ group rotamer.
2. Distinct magnetic environments at each site occupied by a $CH_2D$ group proton.

Previous studies indicate that a nitrogen lone pair neighbouring a $CH_2D$ group can cause relatively large isotope effects on the conformational equilibria [33–35]. Anet and Kopelevich investigated the proton NMR spectrum of racemic *N*-$CH_2D$-2-methylpiperidine, a chiral six-membered ring containing an *N*-$CH_2D$ group, which exhibits a noticeable $CH_2D$ proton chemical shift difference of 14 ppb at 22 °C [25,27–29,31]. This system was then used to assign the configuration of chiral methyl groups by differentiating the tritium NMR signals arising from *N*-CHDT groups [36].

To illustrate how the equilibrium isotope effect (EIE) develops into a substantial rotameric population asymmetry, the three $CH_2D$ rotamers of *N*-$CH_2D$-2-methylpiperidine are considered in Figure 1. The notation for labelling each rotamer follows that set out by O'Leary [28]:

- **S**. The deuteron is sterically interacting with the 2-position $CH_3$ group.
- **F**. The deuteron is free from interaction with the 2-position $CH_3$ group.
- **A**. The deuterium is *anti* to the lone pair of electrons on the nitrogen atom.

The zero-point vibrational energy (ZPVE) for the *N*-methyl C-H(D) bonds in *N*-$CH_2D$-2-methylpiperidine increases when positioned in an *anti* conformation with respect to the adjacent nitrogen lone pair. This zero-point vibrational destabilization arises from C-H/D bond weakening caused by delocalization of the lone pair into the C-H(D) sigma antibonding orbital, i.e., the $n$-$\sigma^*$ hyperconjugation effect [25,27–29,31]. However, the magnitude of destabilization is greater for *anti* C-D bonds over C-H bonds, giving rise to an EIE that partitions the C-D bond preferentially into the gauche positions, i.e., rotamers **S** and **F** are thermodynamically preferred over rotamer **A**. A small steric isotope effect additionally causes a slight preference for the C-D bond to be in proximity with the adjacent 2-substituents such as a methyl group.

Hyperconjugation-associated delocalization energies can be estimated computationally using the natural bond orbital (NBO) approach of Weinhold and co-workers [37]. The NBO analysis transforms the canonical molecular orbitals and non-orthogonal atomic orbitals into localized natural atomic, hybrid and bond orbitals. Filled NBOs then represent the localized Lewis structure of a molecule, and the interactions between filled and antibonding orbitals represent deviations from the ideal Lewis structure and estimates

of the electron delocalization energy (E(2)) can be made using second-order perturbation theory [38]. These energies are readily obtained using NBO Version 3.1 [39] as implemented in *Gaussian 16* [40]. To obtain near-zero delocalization energies, the default E(2) threshold value (0.5 kcal mol$^{-1}$) was adjusted to 0.001 kcal mol$^{-1}$. This was accomplished using the *Gaussian* keyword POP=NBOREAD and the input file was terminated with the line \$NBO E2PERT = 0.001 \$END.

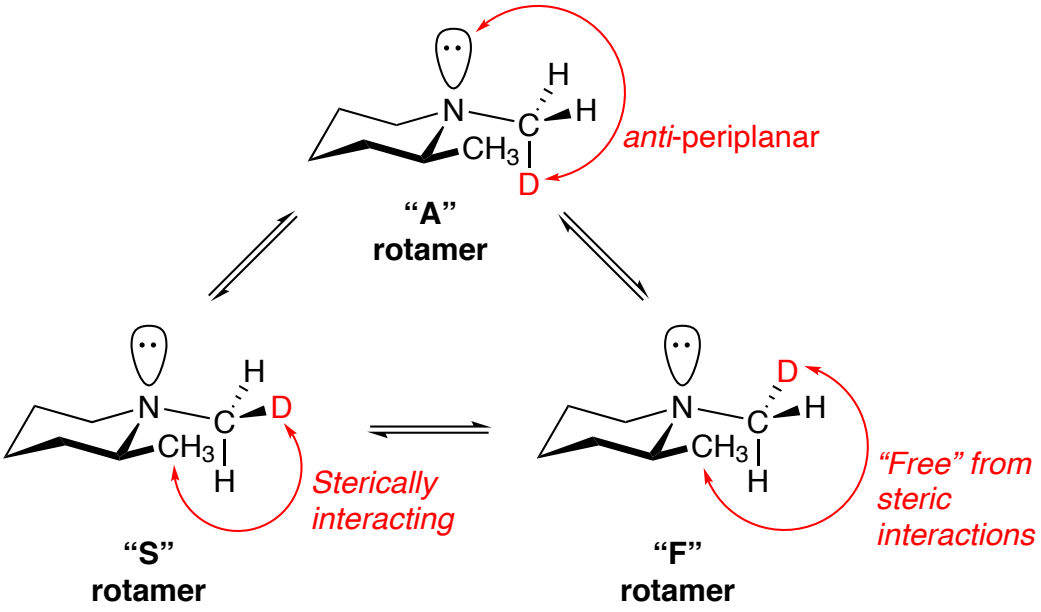


**Figure 1.** The three interchangeable $CH_2D$ rotamers of *N*-$CH_2D$-2-methylpiperidine. **S**: D is sterically hindered; **F**: D is free from interaction; and **A**: D is anti to the nitrogen lone pair.

To assess N(lp)/CH $\sigma^*$ hyperconjugation in *N*-methyl-2-methylpiperidine, the geometry of the diequatorial conformer was optimized and NBOs were computed using B3LYP/6-31G(d,p) density functional theory (see the Electronic Supplementary Information (ESI) for more details). The N(lp)/CH $\sigma^*$ delocalization energies in the optimized geometry are 1.29 kcal mol$^{-1}$ (N(lp)/$CH_{21/S}$), 8.12 kcal mol$^{-1}$ (N(lp)/$CH_{22/A}$) and 0.73 kcal mol$^{-1}$ (N(lp)/$CH_{23/F}$), respectively. The larger delocalization energy for the orbitals involving $H_{22/A}$ is due to effective orbital overlap when the lone pair is anti to the CH $\sigma^*$ orbital, see Figure 2a. Its magnitude, ca. 8 kcal mol$^{-1}$, is similar to a value reported for the same orbital interaction in methylamine [38,41].

A B3LYP/6-31G(d,p) dihedral angle scan and NBO analysis was used to investigate N(lp)/CH $\sigma^*$ hyperconjugation as a function of *N*-$CH_3$ bond rotation (see the ESI for more details). The relaxed scan explored 360° about the $C_4$-$N_{19}$-$C_{20}$-$H_{21}$ dihedral angle $\theta$ in 10° increments using the previously described optimized geometry as a starting structure, see Figure 2b. Single point NBO calculations for each structure on the potential energy surface were then calculated and tabulated as a function of $\theta$, see Figure 2c.

As expected, a delocalization energy maximum (ca. 8 kcal mol$^{-1}$) is observed for an anti-orientation of N(lp)/C-$H_{21}$ $\sigma^*$. A smaller maximum (ca. 4 kcal mol$^{-1}$) is observed for the syn orbital orientation. Arising in eclipsed transition state structures, this hyperconjugation interaction is not relevant to the EIE, which involves only ground state structures. The rotational analysis reveals that the delocalization energy is much smaller (ca. 1 kcal mol$^{-1}$) for gauche orientations of the lone pair and the C-H $\sigma^*$ orbitals.

The EIE is responsible for the observable chemical shift difference $\Delta\nu_{12}$ between the two $CH_2D$ protons of *N*-$CH_2D$-2-methylpiperidine. The approach detailed below is used to predict the magnitude of the chemical shift difference $\Delta\nu_{12}$ for $CH_2D$ protons in a local chiral environment:

1. Compute $\Delta G(i)$ and the relative populations $P(i)$ of the rotamers $i$ = **S**, **F** and **A**.

2. Determine the chemical shift difference $\Delta\nu_{12}(i)$ between the $CH_2D$ protons of the rotamers $i$ = **S**, **F** and **A**.
3. Weight the chemical shift difference $\Delta\nu_{12}(i)$ of each rotamer by the corresponding relative population $P(i)$.

The relative rotamer population $P(i)$ is:

$$P(i) = \frac{e^{\frac{-\Delta G(i)}{k_B T}}}{Z}, \quad (1)$$

where $\Delta G(i)$ is the difference in the Gibbs free energies between C-H and C-D bonds for a given rotamer $i$ [42], $k_B$ is the Boltzmann constant, $T$ is the temperature and $Z$ is a partition function. The partition function is:

$$Z = \sum_i e^{\frac{-\Delta G(i)}{k_B T}}, \quad (2)$$

i.e., the sum of all relative rotamer populations.

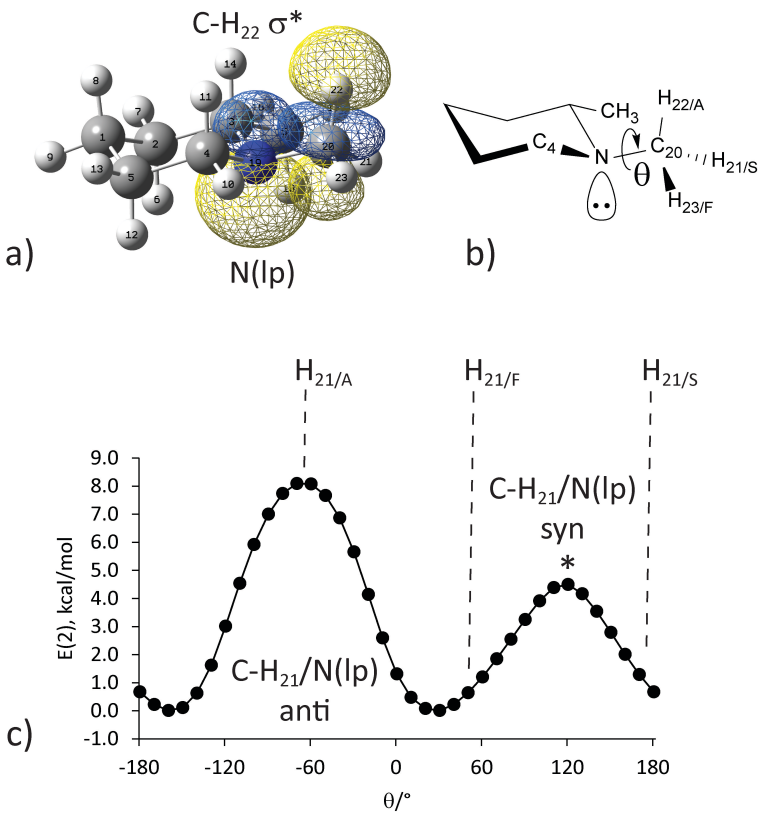


**Figure 2.** (**a**) B3LYP/6-31G(d,p) optimized structure of *N*-methyl-2-methylpiperidine showing localized natural bond orbitals: the non-bonding nitrogen lone pair orbital and the antibonding $\sigma^*$ orbital situated *anti* to it. (**b**) Dihedral angle ($\theta/^\circ$) definition ($C_4$-$N_{19}$-$C_{20}$-$H_{21}$). (**c**) N(lp)/C-$H_{21}$ $\sigma^*$ delocalization energies (kcal $mol^{-1}$) for structures from a relaxed B3LYP/6-31G(d,p) scan (360°, 10° increments) starting with the optimized structure in (**a**).

The method results in the following expression for the chemical shift difference $\Delta\nu_{12}$ between $CH_2D$ group protons:

$$\Delta\nu_{12} = P(\mathbf{S})\Delta\nu_{12}(\mathbf{S}) + P(\mathbf{F})\Delta\nu_{12}(\mathbf{F}) + P(\mathbf{A})\Delta\nu_{12}(\mathbf{A}). \quad (3)$$

The proton chemical shift differences are averaged over all populated $CH_2D$ rotamers, which results in a small $CH_2D$ chemical shift difference $\Delta\nu_{12}$ observable in the $^1H$ NMR spectrum, see Section 3.

### 2.2. Illustrative Examples

Figure 3a displays three molecular candidates which contain a $CH_2D$ group of similar type. Figure 3b shows the **S**, **F** and **A** rotamer populations for the same ring systems (see the ESI for more details). In the cases of *N*-$CH_2D$-2-methylpiperidine and *N*-$CH_2D$-3-methylpiperidine, the lone pair of the adjacent nitrogen atom causes a significant perturbation to the conformational equilibria, as discussed above, and as a result; there is a clear non-uniformity in the $CH_2D$ rotamer populations, i.e., rotameric symmetry breaking. In fact, these two systems have very similar populations for each rotamer, the difference reflecting the aforementioned steric isotope effect favouring placement of a C-D bond in proximity to the 2-methyl substituent. In the case of $CH_2D$-2-methylcyclohexane, the lack of a nitrogen lone pair considerably equalizes the rotamer populations, i.e., the *anti* rotamer **A** is not sufficiently underpopulated with respect to the **S** and **F** rotamers.

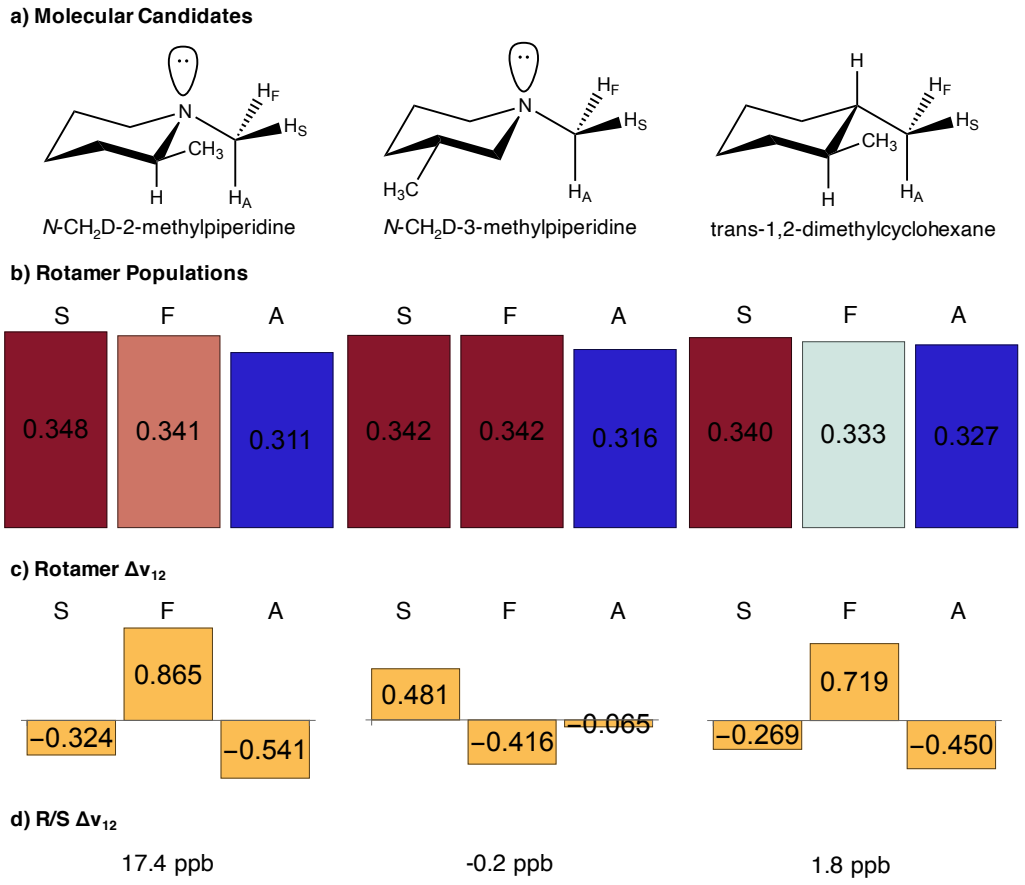


**Figure 3.** (**a**) Molecular candidates chosen to demonstrate the key chemical features of *N*-$CH_2D$-2-methylpiperidine which engender an observable $CH_2D$ chemical shift difference. (**b**) Populations of the **S**, **F** and **A** rotamers for each molecular candidate. (**c**) $CH_2D$ chemical shift differences of the **S**, **F** and **A** rotamers for each molecular candidate given in ppm. Populations are normalized to 1, with values rounded to three decimals places. (**d**) R/S chemical shift difference $\Delta\nu_{12}$ after averaging over all populated states given in ppb.

Figure 3c shows the chemical shift difference between the two $CH_2D$ proton sites for each rotamer indicated in Figure 3b (see the ESI for more details). A distinguishable chemical shift difference for the proton pair in *N*-$CH_2D$-2-methylpiperidine is clearly observable for each rotamer, with the chemical shift difference allowed to be negative in

some cases. The same is true for the **S** and **F** rotamers of *N*-$CH_2D$-3-methylpiperidine, which has an equatorial and significantly more distant 3-position substituent, but with the **A** rotamer not able to forge any substantial chemical shift difference between the two proton sites. Crucially, the two chemical shift differences created by rotamers **S** and **F** are, for all intents and purposes, equal and opposite. Combined with very similar populations for these two rotamers, this essentially wipes out any observable $CH_2D$ chemical shift difference for *N*-$CH_2D$-3-methylpiperidine, see Figure 3d. After averaging over all populated states, the $CH_2D$ chemical shift difference for this molecular system is predicted to be just -0.2 ppb. This simple example clearly demonstrates the importance that the proximal methyl group plays in the observable $CH_2D$ proton chemical shift difference of *N*-$CH_2D$-2-methylpiperidine.

The proximal 2-methyl group of $CH_2D$-2-methylcyclohexane brings about rotameric $^1H$ chemical shift differences which are similar to those of *N*-$CH_2D$-2-methylpiperidine, as required for an observable $CH_2D$ chemical shift difference. Detrimentally, the relatively flat distribution of rotamer populations does not favourably weight the chemical shift difference of each rotamer in the same way as *N*-$CH_2D$-2-methylpiperidine. Consequently, a $CH_2D$ proton chemical shift difference of just 1.8 ppb is predicted for this system, after averaging over all populated states. This indicates that forging a substantial rotamer population imbalance is just as critical as creating large rotameric chemical shift differences in preparing an appreciable $CH_2D$ group chemical shift difference, and that ultimately both effects are required simultaneously. However, some 2-substituted groups are less suitable in creating rotameric chemical shift differences than others. This point is highlighted below in Section 5.

### *2.3. The Role of Nitrogen*

It has been previously highlighted that except in unusual circumstances for the case of a transition metal complex [26] or a system containing an intramolecular C-H(D)- - -N hydrogen bond [27,28], the previous instances of observable $CH_2D$ proton chemical shift differences have been engendered by an $n$-$\sigma^*$ hyperconjugation interaction involving the lone pair of electrons belonging to an atom of nitrogen [25,29,31]. Clearly, the nitrogen atom plays a key role in this phenomenon. In a previous article [29], we suggested that "experiments could be attempted on chiral substances accommodating an X-$CH_2D$ moiety, where X is S, P or O, i.e., an atom possessing a lone pair, other than nitrogen".

Rather than synthesizing suitable molecular derivatives, we have computed the $CH_2D$ rotamer populations in these compounds. In all cases, a relatively flat $CH_2D$ population distribution is calculated. In 1,2-dimethylphosphinane, the phosphorus analogue of *N*-methyl-2-methylpiperidine, the $CH_2D$ population distribution is $\{P(\mathbf{S}) = 0.337, P(\mathbf{F}) = 0.333, P(\mathbf{A}) = 0.330\}$ and since no one rotamer is significantly disfavoured, as in the case of *N*-$CH_2D$-2-methylpiperidine, an appreciable $CH_2D$ chemical shift difference is unlikely to be engendered between the two proton sites after averaging over all populated states (see the ESI for more details). This is due to an attenuated orbital interaction between the phosphorus lone pair and the anti C-H $\sigma^*$ orbital.

Regarding *S*-$CH_2D$ groups, it is worth nothing that an experimental attempt to observe the small chemical shift difference between the $CH_2D$ proton sites of $CH_2D$-*S*-adenosylmethionine was unsuccessful, likely because $\Delta\nu_{12}$ was too small to observe in this case. Other *N*-, *O*- and *S*-$CH_2D$ derivatives which do not show an appreciable proton chemical shift difference are found in the PhD thesis of O'Leary [43].

## 3. $^1H$ NMR Spectrum

The methyl group region of the experimental $^1H$ NMR spectrum of *N*-$CH_2D$-2-methylpiperidine is shown in Figure 4. This spectral portion has the characteristic AB appearance of a marginally inequivalent proton pair when a $^2H$ radiofrequency field is applied to remove the $^2J_{HD}$ couplings, indicating a small chemical shift difference with respect to the in-pair scalar coupling. The two central peaks of the AB spectral pattern are resolved,

and are separated by an inner splitting of ∼1.8 Hz. The spectrum is consistent with and is simulated using a $J$-coupling of $|J_{12}| = 11.7 \pm 0.2$ Hz and a chemical shift difference of $\Delta\nu_{12} = 13.5 \pm 0.6$ ppb between the $CH_2D$ proton sites, as reported previously [25].

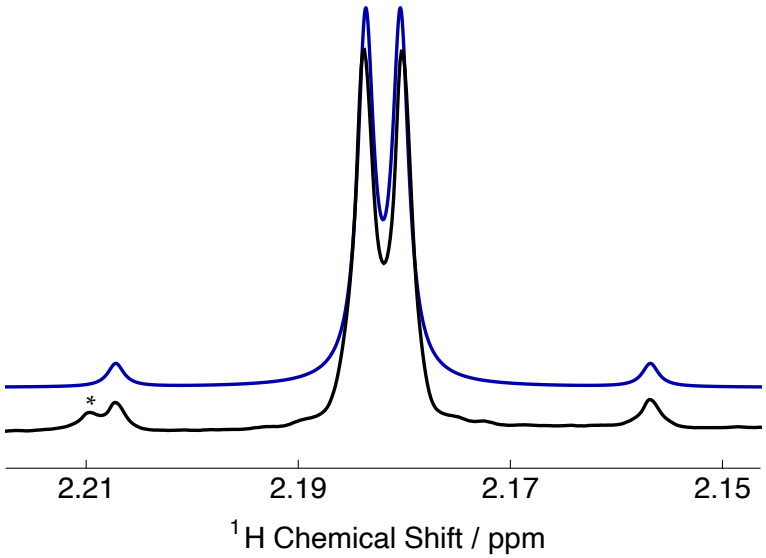


**Figure 4.** Relevant portion of the experimental $^1$H NMR spectrum of 0.1 M $N$-$CH_2D$-2-methylpiperidine dissolved in $CD_2Cl_2$ solvent acquired at 11.75 T ($^1$H nuclear Larmor frequency = 500 MHz) and 25 °C with a single transient in the presence of $^2$H decoupling (deuteron nutation frequency = 500 Hz). Black line: Experimental spectrum; Blue line: Simulated spectrum ($|J_{12}|$ = 11.7 Hz, $\Delta\nu_{12} = 13.5$ ppb), using Lorentzian line broadening (half-width at half-height = 0.9 Hz). Simulations were performed using the *Mathematica*-based NMR software package *SpinDynamica* [44]. The asterisk denotes a small peak from a non-deuterated $N$-$CH_3$-2-methylpiperidine impurity, shifted in frequency by a small intrinsic isotope effect.

## 4. Environmental Influences

The size of the chemical shift difference $\Delta\nu_{12}$ in the $N$-$CH_2D$ group of $N$-$CH_2D$-2-methylpiperidine is influenced by experimental factors such as temperature and solvent. The populations of the rotamers **S**, **F** and **A** are clearly dependent on temperature, as given by Equation (1). Figure 5a shows these rotamer populations over a range of temperatures which are easily accessible by a liquid-state NMR probe. Consistent with elementary Boltzmann physics, the rotamer populations become increasingly more equal as the temperature increases. Rotamers **S** and **F** are initially overpopulated due to the influence the $n$-$\sigma^*$ hyperconjugation interaction with the nitrogen lone pair has on the conformational equilibria, with these rotamers consequently becoming less populated as the temperature increases. The opposite effect is observed for the **A** rotamer population, which was initially underpopulated due to the decreased zero-point vibrational stabilization, and becomes more populated at elevated temperatures. It is interesting to note that the rotamer which was initially populated furthest away from its equilibrium value gains population more quickly with increasing temperature. The blue curve in Figure 5a shows an increase in the **A** rotamer population of ∼0.54% over the range of temperatures explored. The population shifts follow the exponential behaviour given by Equation (1).

Figure 5b shows the influence of temperature on the chemical shift difference $\Delta\nu_{12}$. The chemical shift difference decreases linearly as the temperature is increased, which is in line with the values of the relative rotamer populations converging at higher temperatures. An analogous trend was observed experimentally [29]. In the limit of increasing temperature, the three rotamer populations would continue to equalize, which would lead to a smaller, and eventually zero, $CH_2D$ proton chemical shift difference. The $CH_2D$ chemical shift difference will be considerably larger at lower temperatures, as was observed by

Anet and Kopelevich when studying the experimental $^1$H NMR spectrum of *N*-$CH_2$D-2-methylpiperidine at −95 °C [25]. It is striking that such a relatively small change in the population of the **A** rotamer, and simultaneously the **S** and **F** rotamers, leads to a much more significant change in $\Delta\nu_{12}$ over the same range of temperatures, with the size of $\Delta\nu_{12}$ decreasing by ∼9.4%.

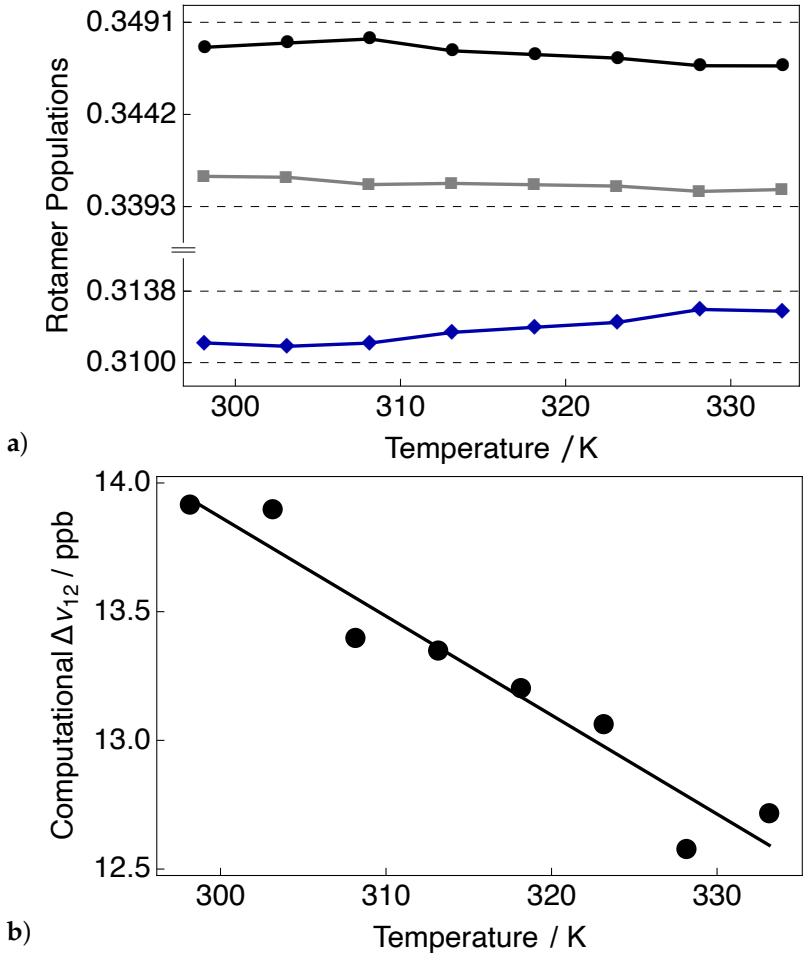


**Figure 5.** (**a**) Populations of the $CH_2D$ rotamers **S** (black filled circles), **F** (grey filled squares) and **A** (blue filled diamonds) as a function of temperature. (**b**) Computational chemical shift difference $\Delta\nu_{12}$ between the $CH_2D$ protons of *N*-$CH_2$D-2-methylpiperidine as a function of temperature.

The lone pair situated on the nitrogen atom is exposed, and as such can be readily protonated by $H^+$ ions in solution. It is hypothesized that since the lone pair plays such a crucial role in the $n$-$\sigma^*$ hyperconjugation interaction, protonation of this site will quench the $CH_2D$ proton chemical shift difference in *N*-$CH_2$D-2-methylpiperidine. This was demonstrated in early studies of *N*-$CH_2$D-2-methylpiperidine [43]. Figure 6 shows $\Delta\nu_{12}$ as a function of the trifluoroacetic (TFA) acid equivalency in solution, i.e., an acid equivalency of 100% indicates a 1:1 ratio of *N*-$CH_2$D-2-methylpiperidine to TFA acid. A linear decrease in $\Delta\nu_{12}$ is observed with increasing acid equivalency. The chemical shift difference does not quite reach 0 ppb at 100% acid equivalency, indicating that perhaps not all the *N*-$CH_2$D group lone pairs have been protonated, but $\Delta\nu_{12}$ could be completely removed by adding excess acid to the solution. This preliminary work opens up the possibility to use *N*-$CH_2$D-2-methylpiperidine as a pH sensitive LLS sensor. We hope to exploit this phenomenon in a future publication.

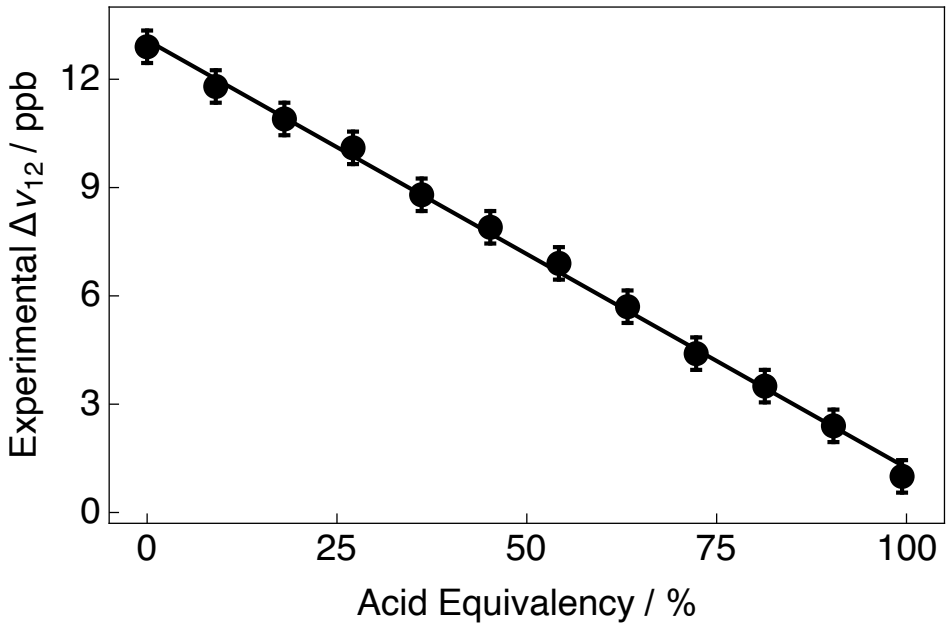


**Figure 6.** Experimental chemical shift difference $\Delta\nu_{12}$ between the $CH_2D$ protons of 0.1 M *N*-$CH_2D$-2-methylpiperidine dissolved in $CDCl_3$ solvent acquired at 11.75 T ($^1H$ nuclear Larmor frequency = 500 MHz) and 25 °C as a function of trifluoroacetic (TFA) acid molar equivalents added to solution.

## 5. Tuning $\Delta\nu_{12}$

Little was previously known regarding the properties of the 2-substituent group required to forge the $CH_2D$ chemical shift difference and control its magnitude. Encouraged by previous results [25–30], a variety of 2-substituted piperidine derivatives were explored with the goal of understanding how the steric and electronic nature of these groups perturbs the EIE and in turn the $CH_2D$ chemical shift difference. The previous study into how the size and properties of the 2-position substituent on the piperidine ring influences the $CH_2D$ proton chemical shift difference was performed by Ogba et al. [31]. A brief review of such findings is presented in Figure 7, which shows the computed $CH_2D$ chemical shift differences compared to experimental findings. The fit of a straight line to the data with a slope of 1 and zero intercept is remarkably good. The only point which partially deviates from the fit to the data is for *N*-$CH_2D$-2-ethynylpiperidine ($\Delta\nu_{12}$ = 4.7 ppb). For this system, the dominant conformation (>99%) in solution is eq-$CH_2D$-ax-2-ethynylpiperidine (eq = equatorial, ax = axial), i.e., the 2-ethynyl substituent occupies the axial position. The same is true for the major fractional population of *N*-$CH_2D$-2-phenylpiperidine, for which a relatively small value of $\Delta\nu_{12}$ = 0.3 ppb was computed.

Building upon previously established methods for predicting the size of $^1H$ chemical shift differences in piperidine derivatives with *N*-$CH_2D$ groups, it was found that in the family of compounds studied the primary governing influence was the preferred stereoisomeric relationship of the $CH_2D$ group with the 2-substituent. Non-polar and large 2-substituents favour the (di-)equatorial position and produce relatively large $CH_2D$ proton chemical shift differences, often exceeding 13 ppb. For polar and smaller groups, a shift towards the eq-$CH_2D$-ax-2-R-piperidine conformation, where R is a polar or small 2-substituent, is preferred due to anomeric effects [45], which stabilizes axial polar bonds at the 2-position by the interaction of their antibonding orbitals with the nitrogen lone pair. The previous study was comprehensively expanded compared with prior investigations [28], and in each piperidine species considered all four possible axial/equatorial conformations before computing a weighted average of the chemical shift differences over all populated states.

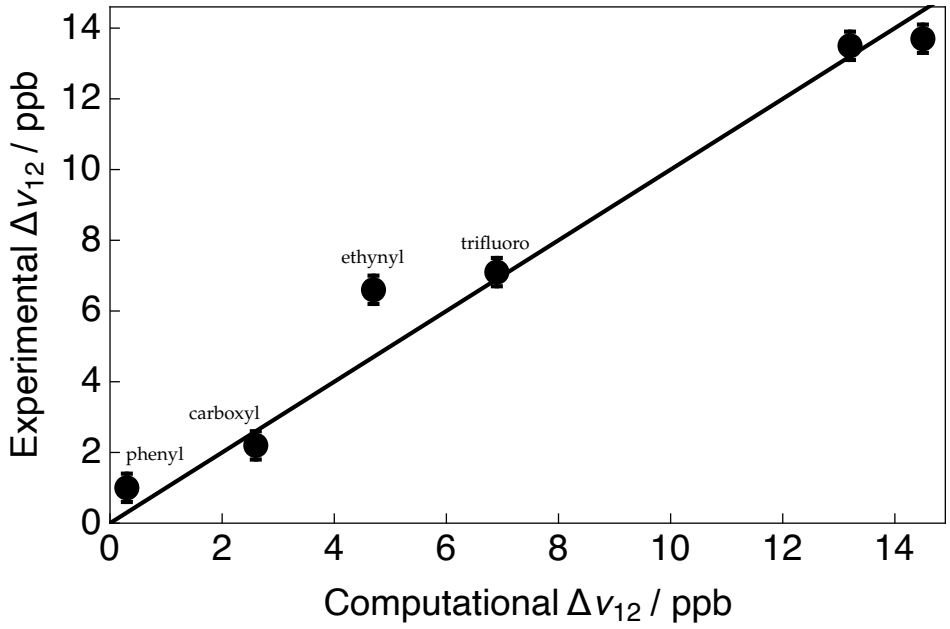


**Figure 7.** Computational vs. experimental chemical shift difference between the $CH_2D$ protons of *N*-$CH_2D$-2-x-piperidine, where x is the chosen 2-substituent group. 2-position substituents of interest are labelled (see the main text for more details). The black line indicates a straight line fit to the data with a slope of 1 and zero intercept.

Some interesting effects were unveiled for a few of the more exotic piperidine derivatives. In the case of *N*-$CH_2D$-2-trifluoropiperidine, a stabilizing hyperconjugation interaction between the nitrogen atom lone pair and the 2-position anti C-C $\sigma^*$ orbital leads to a distribution in the dominant fractional populations between the eq-$CH_2D$-eq-2-R (57%) and eq-$CH_2D$-ax-2-R (35%) conformations. A weakened rotameric asymmetry, due to a diminished lone pair-$CH_2D$ interaction, results in a smaller proton chemical shift difference between the $^1H$ sites ($\Delta\nu_{12}$ = 6.9 ppb).

The magnitude of the computed and experimentally observed values of $\Delta\nu_{12}$ for methyl 1-($CH_2D$)-piperidine-2-carboxylate ($\Delta\nu_{12}$ = 2.6 ppb) are relatively small compared with the above described *N*-$CH_2D$-2-trifluoropiperidine ($\Delta\nu_{12}$ = 6.9 ppb), which displays a similar set of dominant fractional populations of stereoisomers [31]. The origin of this deviation for the 2-ester substituted piperidine derivative was realized by ascribing a CH···O interaction [46–49] between the ester carboxyl oxygen and the proximal *N*-methyl H(D), which contributes to deshielding effects at the S position, and produces a small difference in shielding constants between a single proton in the **S** and **F** rotamers since the overall difference in magnetic environments for the two protons in the $CH_2D$ pair is reduced [50].

To illustrate the magnitude of the methyl positional $^1H$ chemical shift differences, we have investigated the *N*-$CH_3$ shielding behaviour in the diequatorial conformation of methyl 1-methylpiperidine-2-carboxylate as a function of side chain rotation, using an approach for calculating accurate $^1H$ chemical shifts, see Figure 8 [51,52]. In this approach, structures are first optimized in the gas phase using B3LYP/6-31G(d) density functional theory, followed by NMR Gauge-Independent Atomic Orbital (GIAO) calculations in a chloroform solvent continuum using the WP04 density functional and the cc-PVTZ basis set (see the ESI for more details). We followed this protocol after first identifying two minimum energy structures (GS1 and GS2) on a potential energy surface defined by a relaxed side chain dihedral angle scan. This procedure directly reveals the $^1H$ chemical shifts, which are obtained by scaling the shielding values *m* according to the equation: $\delta\,^1H = (31.8444 - m)/1.0205$. Our previous work [31] took the same general approach, albeit in a

$CH_2Cl_2$ solvent continuum to align results with experimental data, and with subtraction of tetramethylsilane $^1H$ shielding values to produce chemical shifts.

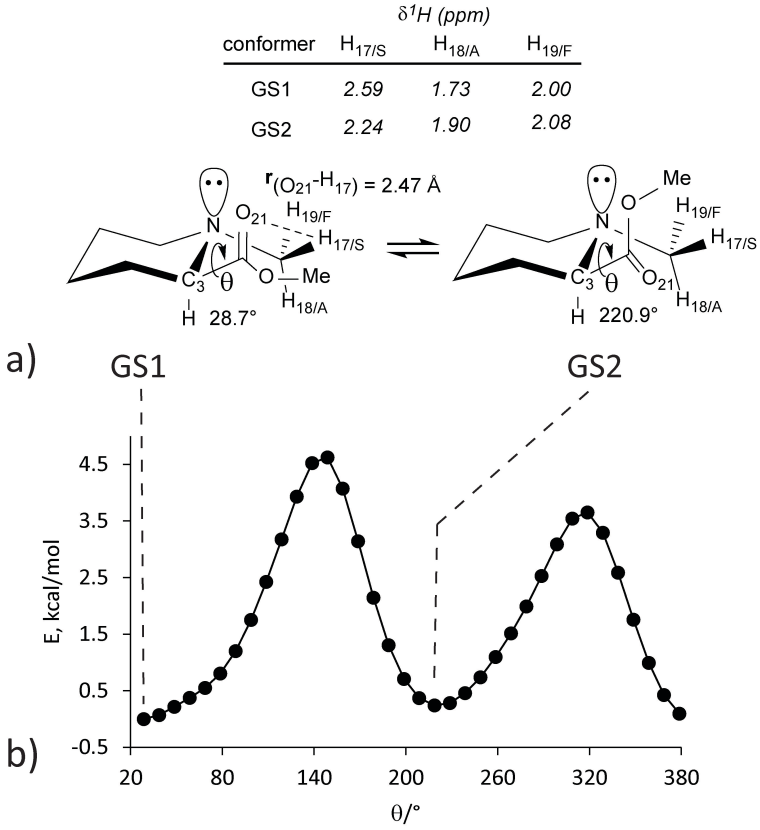


**Figure 8.** (**a**) *N*-$CH_3$ bond definitions, principal side chain ground state conformers (GS1 and GS2) of methyl 1-methylpiperidine-2-carboxylate and dihedral angle ($\theta/°$) definition (N-$C_3$-$C_{20}$-$O_{21}$). $\theta$ values (28.7° and 220.9°) obtained from B3LYP/6-31G(d) optimized structures, and WP04/cc-PVTZ (PCM: $CHCl_3$) $^1H$ NMR chemical shifts (ppm). (**b**) Relaxed B3LYP/6-31G(d) potential energy scan (360°, 10° increments) starting with optimized GS1 structure in (**a**).

The side chain dihedral scan of methyl 1-methylpiperidine carboxylate identified two minima, with a lower-energy ground state (GS1) separated from the other (GS2) by ca. 0.24 kcal $mol^{-1}$ in terms of their electronic energies. After inclusion of vibrational enthalpy and entropy contributions, the adjusted energy difference corresponds to a 4:1 ratio of the two forms at 298 K. The aforementioned CH···O interaction is demonstrated in the major conformer (GS1) by a close contact (2.47 Å) between the ester carbonyl $O_{21}$ and the proximal $H_{17/S}$. The calculated chemical shift of $H_{17/S}$ in GS1 is 2.59 ppm, which is deshielded by 0.35 ppm in comparison to same site in conformer GS2. There are also smaller shift differences for $H_{18/A}$ in the two conformers, with this position more shielded in GS1 (1.73 ppm) than in GS2 (1.90 ppm). The shifts at $H_{19/F}$ differ even less (GS1: 2.00 ppm, GS2: 2.08 ppm), a consequence of these C-H bonds projecting into similar magnetic environments.

## 6. $CH_2D$ LLS

Access to methyl group LLS were previously achieved by executing exotic NMR experiments involving the dissolution of material from cryogenic conditions [53–56]. In these cases, the methyl groups also required an additional nuclear spin ($^{13}C$) which engendered LLS readout via inefficient cross-relaxation processes, which significantly diminished the available intensity of the observable $^1H$ NMR signal.

To demonstrate the feasibility of accessing LLS in monodeuterated methyl groups, the LLS of the proton pair in the *N*-$CH_2D$ group of *N*-$CH_2D$-2-methylpiperidine was shown to be populated due to the presence of the small $CH_2D$ proton chemical shift difference [29].

The LLS lifetimes $T_S$ approached ~1 min at elevated temperatures, with the ratio of the LLS relaxation time constant $T_S$ to the longitudinal relaxation time constant $T_1$ observed to be exceptionally constant over a wide range of experimental conditions and equal to $3.2 \pm 0.1$ [4].

## 7. Conclusions

Non-uniformity, i.e., symmetry breaking, in the rotamer populations of *N*-$CH_2D$-2-methylpiperidine combined with a local chiral environment allows access to diastereotopic methyl hydrogens and $CH_2D$ group LLS. A hyperconjugation interaction involving the nitrogen lone pair perturbs the vibrational energies and hence the rotamer populations, while the proximal methyl group creates a chiral environment, and combine to engender a small isotropic chemical shift difference between the $CH_2D$ proton sites, which is clearly observable in the experimental $^1$H NMR spectrum. The magnitude of the $CH_2D$ chemical shift difference was explored as a function of environmental factors such as temperature and acidity, as well as the motion and type of molecular substituents at the 2-position on the piperidine ring. Stereoelectronic effects of the 2-substituents strongly affect the proton chemical shift difference, with the polarity and size of the 2-substituent affecting the 1,2-stereoisomeric relationship, and as a result; the influence of the rotational asymmetry within the $CH_2D$ group.

**Supplementary Materials:** The following are available online at https://www.mdpi.com/article/10.3390/sym13091610/s1, Figure S1. $C_4$-$N_{19}$-$C_{20}$-$H_{21}$ reference atoms used for defining dihedral angle q for B3LYP/6-31G(d,p) relaxed scan of methyl rotation in *N*-methyl-2-methylpiperidine. Figure S2. Methyl numbering scheme for (l-r): *N*-methyl-2-methylpiperidine, *N*-methyl-3-methylpiperidine and trans-1,2-dimethylcyclohexane. Figure S3. Methyl numbering scheme for 1,2-dimethylphosphinane. Figure S4. $N_{15}$-$C_3$-$C_{20}$-$O_{21}$ reference atoms used for defining dihedral angle q for B3LYP/6-31G(d) relaxed scan of ester rotation in methyl 1-methylpiperidine carboxylate. Table S1. B3LYP/6-31G(d,p) Optimized Coordinates for *N*-Methyl-2-Methylpiperidine. Table S2. B3LYP/6-31G(d,p) N(lp)→CH s* delocalization energies (kcal/mol) in *N*-methyl-2-methylpiperidine. Table S3. wB97x/cc-PVTZ Optimized Coordinates for *N*-Methyl-2-Methylpiperidine. Table S4. wB97x/cc-PVTZ Optimized Coordinates for *N*-Methyl-3-Methylpiperidine. Table S5. wB97x/cc-PVTZ Optimized Coordinates for trans-1,2-dimethylcyclohexane. Table S6. Boltzmann Population and pro-R and pro-S Chemical Shift Analysis for *N*-methyl-2-methylpiperidine. Table S7. Boltzmann Population and pro-R and pro-S Chemical Shift Analysis for *N*-methyl-3-methylpiperidine. Table S8. Boltzmann Population and pro-*R* and pro-*S* Chemical Shift Analysis for trans-1,2-dimethylcyclohexane. Table S9. B3LYP/6-31G(d,p) Optimized Coordinates for 1,2-dimethylphosphinane. Table S10. Boltzmann Population Analysis for 1,2-dimethylphoshinane. Table S11. B3LYP/6-31G(d,p) P(lp)→CH σ* delocalization energies (kcal/mol) in 1,2-dimethylphosphinane. Table S12. B3LYP/6-31G(d) Optimized Coordinates for Methyl 1-Methylpiperidine Carboxylate (GS1 Conformation). Table S13. B3LYP/6-31G(d) conformational energies (kcal/mol) for ester rotation in methyl 1-methylpiperidine carboxylate. Table S14. B3LYP/6-31G(d) Optimized Coordinates for Methyl 1-Methylpiperidine Carboxylate (GS2 Conformation). Table S15. WP04/cc-PVDZ (PCM = chloroform) $^1$H NMR shielding values and calculated chemical shifts in the GS1 and GS2 conformers of methyl 1-methylpiperidine carboxylate.

**Author Contributions:** S.J.E. carried out the experiments, performed the computations, analyzed the data and co-wrote the manuscript; O.M.O. performed the computations, analyzed the data and co-wrote the manuscript; L.J.B. synthesized the molecular candidates employed in this study; and D.J.O. performed the computations, analyzed the data and co-wrote the manuscript. All authors have read and agreed to the published version of the manuscript.

**Funding:** This research was supported by the Engineering and Physical Sciences Research Council (UK), grant codes EP/N002482 and EP/L505067/1, the Leverhulme Trust, grant code RPG-2020-066, the Wolfson Foundation, the Royal Society/CNRS exchange scheme and by Bruker Biospin (USA).

**Data Availability Statement:** Data are available upon request from the corresponding authors.

**Acknowledgments:** S.J.E. would like to acknowledge Gabriele Stevanato for providing the opportunity to contribute this article, Jean-Nicolas Dumez for assistance with modelling relaxation data,

Malcolm H. Levitt for enlightening discussions and Frédéric Blanc for providing support, guidance and encouragement. D.J.O. thanks Pomona College for financial support.

**Conflicts of Interest:** The authors declare no competing interest.

## References

1. Carravetta, M.; Johannessen, O.G.; Levitt, M.H. Beyond the $T_1$ Limit: Singlet Nuclear Spin States in Low Magnetic Fields. *Phys. Rev. Lett.* **2004**, *92*, 153003. [CrossRef] [PubMed]
2. Levitt, M.H. Singlet Nuclear Magnetic Resonance. *Annu. Rev. Phys. Chem.* **2012**, *63*, 89–105. [CrossRef]
3. Levitt, M.H. Long live the singlet state! *J. Magn. Reson.* **2019**, *306*, 69–74. [CrossRef] [PubMed]
4. *Long-Lived Nuclear Spin Order*; New Developments in NMR; The Royal Society of Chemistry: London, UK, 2020; pp. 1–441. [CrossRef]
5. Pileio, G.; Carravetta, M.; Hughes, E.; Levitt, M.H. The Long-Lived Nuclear Singlet State of $^{15}$N-Nitrous Oxide in Solution. *J. Am. Chem. Soc.* **2008**, *130*, 12582–12583. [CrossRef]
6. Dumez, J.N.; Hill-Cousins, J.T.; Brown, R.C.D.; Pileio, G. Long-lived localization in magnetic resonance imaging. *J. Magn. Reson.* **2014**, *246*, 27–30. [CrossRef] [PubMed]
7. Pileio, G.; Dumez, J.N.; Pop, I.A.; Hill-Cousins, J.T.; Brown, R.C.D. Real-space imaging of macroscopic diffusion and slow flow by singlet tagging MRI. *J. Magn. Reson.* **2015**, *252*, 130–134. [CrossRef] [PubMed]
8. Elliott, S.J.; Kadeřávek, P.; Brown, L.J.; Sabba, M.; Glöggler, S.; O'Leary, D.J.; Brown, R.C.D.; Ferrage, F.; Levitt, M.H. Field-cycling long-lived-state NMR of $^{15}N_2$ spin pairs. *Mol. Phys.* **2018**, *117*, 861–867. [CrossRef]
9. Erriah, B.; Elliott, S.J. Experimental evidence for the role of paramagnetic oxygen concentration on the decay of long-lived nuclear spin order. *RSC Adv.* **2019**, *9*, 23418–23424. [CrossRef]
10. Kiryutin, A.S.; Zimmermann, H.; Yurkovskaya, A.V.; Vieth, H.M.; Ivanov, K.L. Long-lived spin states as a source of contrast in magnetic resonance spectroscopy and imaging. *J. Magn. Reson.* **2015**, *261*, 64–72. [CrossRef]
11. Salvi, N.; Buratto, R.; Bornet, A.; Ulzega, S.; Rentero Rebollo, I.; Angelini, A.; Heinis, C.; Bodenhausen, G. Boosting the Sensitivity of Ligand-Protein Screening by NMR of Long-Lived States. *J. Am. Chem. Soc.* **2012**, *134*, 11076–11079. [CrossRef]
12. Bornet, A.; Ji, X.; Mammoli, D.; Vuichoud, B.; Milani, J.; Bodenhausen, G.; Jannin, S. Long-Lived States of Magnetically Equivalent Spins Populated by Dissolution-DNP and Revealed by Enzymatic Reactions. *Chem. A Eur. J.* **2014**, *20*, 17113–17118. [CrossRef]
13. Ardenkjær-Larsen, J.H.; Fridlund, B.; Gram, A.; Hansson, G.; Hansson, L.; Lerche, M.H.; Servin, R.; Thaning, M.; Golman, K. Increase in signal-to-noise ratio of >10,000 times in liquid-state NMR. *Proc. Natl. Acad. Sci. USA* **2003**, *100*, 10158–10163. [CrossRef]
14. Vasos, P.R.; Comment, A.; Sarkar, R.; Ahuja, P.; Jannin, S.; Ansermet, J.P.; Konter, J.A.; Hautle, P.; van den Brandt, B.; Bodenhausen, G. Long-lived states to sustain hyperpolarized magnetization. *Proc. Natl. Acad. Sci. USA* **2009**, *106*, 18469–18473. [CrossRef]
15. Pileio, G.; Bowen, S.; Laustsen, C.; Tayler, M.C.D.; Hill-Cousins, J.T.; Brown, L.J.; Brown, R.C.D.; Ardenkjær-Larsen, J.H.; Levitt, M.H. Recycling and Imaging of Nuclear Singlet Hyperpolarization. *J. Am. Chem. Soc.* **2013**, *135*, 5084–5088. [CrossRef]
16. Elliott, S.J.; Meier, B.; Vuichoud, B.; Stevanato, G.; Brown, L.J.; Alonso-Valdesueiro, J.; Emsley, L.; Jannin, S.; Levitt, M.H. Hyperpolarized long-lived nuclear spin states in monodeuterated methyl groups. *Phys. Chem. Chem. Phys.* **2018**, *20*, 9755–9759. [CrossRef] [PubMed]
17. Pileio, G.; Carravetta, M.; Levitt, M.H. Storage of nuclear magnetization as long-lived singlet order in low magnetic field. *Proc. Natl. Acad. Sci. USA* **2010**, *107*, 17135–17139. [CrossRef]
18. Tayler, M.C.D.; Levitt, M.H. Singlet nuclear magnetic resonance of nearly-equivalent spins. *Phys. Chem. Chem. Phys.* **2011**, *13*, 5556–5560. [CrossRef]
19. Bengs, C.; Sabba, M.; Jerschow, A.; Levitt, M.H. Generalised magnetisation-to-singlet-order transfer in nuclear magnetic resonance. *Phys. Chem. Chem. Phys.* **2020**, *22*, 9703–9712. [CrossRef]
20. Hill-Cousins, J.T.; Pop, I.A.; Pileio, G.; Stevanato, G.; Håkansson, P.; Roy, S.S.; Levitt, M.H.; Brown, L.J.; Brown, R.C.D. Synthesis of an Isotopically Labeled Naphthalene Derivative That Supports a Long-Lived Nuclear Singlet State. *Org. Lett.* **2015**, *17*, 2150–2153. [CrossRef]
21. Stevanato, G.; Hill-Cousins, J.T.; Håkansson, P.; Roy, S.S.; Brown, L.J.; Brown, R.C.D.; Pileio, G.; Levitt, M.H. A Nuclear Singlet Lifetime of More than One Hour in Room-Temperature Solution. *Angew. Chem. Int. Ed.* **2015**, *54*, 3740–3743. [CrossRef]
22. Tayler, M.C.D.; Levitt, M.H. Accessing Long-Lived Nuclear Spin Order by Isotope-Induced Symmetry Breaking. *J. Am. Chem. Soc.* **2013**, *135*, 2120–2123. [CrossRef]
23. Pravdivtsev, A.N.; Sönnichsen, F.D.; Hövener, J.B. In vitro singlet state and zero-quantum encoded magnetic resonance spectroscopy: Illustration with *N*-acetyl-aspartate. *PLoS ONE* **2020**, *15*, e0239982. [CrossRef]
24. Zhang, Y.; Soon, P.C.; Jerschow, A.; Canary, J.W. Long-Lived $^1$H Nuclear Spin Singlet in Dimethyl Maleate Revealed by Addition of Thiols. *Angew. Chem. Int. Ed.* **2014**, *53*, 3396–3399. [CrossRef] [PubMed]
25. Anet, F.A.L.; Kopelevich, M. Detection and assignments of diastereotopic chemical shifts in partially deuteriated methyl groups of a chiral molecule. *J. Am. Chem. Soc.* **1989**, *111*, 3429–3431. [CrossRef]
26. Restelli, A.; Siegel, J.S. Cryptoclastic diastereotopism: NMR evidence for the chirotopicity of the methyl group in (α-deuterio-o-chlorotoluene)chromium tricarbonyl. *J. Am. Chem. Soc.* **1992**, *114*, 1091–1092. [CrossRef]

27. Allen, B.D.; O'Leary, D.J. Fomenting Proton Anisochronicity in the $CH_2D$ Group. *J. Am. Chem. Soc.* **2003**, *125*, 9018–9019. [CrossRef]
28. Allen, B.D.; Cintrat, J.C.; Faucher, N.; Berthault, P.; Rousseau, B.; O'Leary, D.J. An Isosparteine Derivative for Stereochemical Assignment of Stereogenic (Chiral) Methyl Groups Using Tritium NMR: Theory and Experiment. *J. Am. Chem. Soc.* **2005**, *127*, 412–420. [CrossRef]
29. Elliott, S.J.; Brown, L.J.; Dumez, J.N.; Levitt, M.H. Long-lived nuclear spin states in monodeuterated methyl groups. *Phys. Chem. Chem. Phys.* **2016**, *18*, 17965–17972. [CrossRef]
30. Elliott, S.J.; Brown, L.J.; Dumez, J.N.; Levitt, M.H. Long-lived nuclear spin states in rapidly rotating $CH_2D$ groups. *J. Magn. Reson.* **2016**, *272*, 87–90. [CrossRef]
31. Ogba, O.M.; Elliott, S.J.; Kolin, D.A.; Brown, L.J.; Cevallos, S.; Sawyer, S.; Levitt, M.H.; O'Leary, D.J. Origins of Small Proton Chemical Shift Differences in Monodeuterated Methyl Groups. *J. Org. Chem.* **2017**, *82*, 8943–8949. [CrossRef]
32. Binsch, G.; Franzen, G.R. Intrinsically anisochronous nuclei in propeller molecules. *J. Am. Chem. Soc.* **1969**, *91*, 3999–4000. [CrossRef]
33. Anet, F.A.L.; Kopelevich, M. Anomeric and conformational deuterium isotope effects in saturated sulphur and nitrogen heterocycles. *J. Chem. Soc. Chem. Commun.* **1987**, *8*, 595–597. [CrossRef]
34. Forsyth, D.A.; Hanley, J.A. Conformationally dependent intrinsic and equilibrium isotope effects in *N*-methylpiperidine. *J. Am. Chem. Soc.* **1987**, *109*, 7930–7932. [CrossRef]
35. Forsyth, D.A.; Prapansiri, V. Conformational equilibrium isotope effects in 3-azabicyclo[3.2.2]nonanes. *Tetrahedron Lett.* **1988**, *29*, 3551–3554. [CrossRef]
36. Anet, F.A.L.; O'Leary, D.J.; Beale, J.M.; Floss, H.G. Stereogenic (chiral) methyl groups: determination of configuration by direct tritium NMR spectroscopy. *J. Am. Chem. Soc.* **1989**, *111*, 8935–8936. [CrossRef]
37. Weinhold, F.; Landis, C.; Glendening, E. What is NBO analysis and how is it useful? *Int. Rev. Phys. Chem.* **2016**, *35*, 399–440. [CrossRef]
38. Alabugin, I.V.; dos Passos Gomes, G.; Abdo, M.A. Hyperconjugation. *Wiley Interdiscip. Rev. Comput. Mol. Sci.* **2019**, *9*, e1389. [CrossRef]
39. Glendening, E.D.; Reed, A.E.; Carpenter, J.E.; Weinhold, F. *NBO*, Version 3.1; Gaussian Inc.: Pittsburgh, PA, USA, 2003.
40. Frisch, M.J.; Trucks, G.W.; Schlegel, H.B.; Scuseria, G.E.; Robb, M.A.; Cheeseman, J.R.; Scalmani, G.; Barone, V.; Petersson, G.A.; Nakatsuji, H.; et al. *Gaussian 16, Revision C.01*; Gaussian Inc.: Wallingford, CT, USA, 2019.
41. Available online: https://nbo6.chem.wisc.edu/tutorial.html (accessed on 24 May 2021).
42. Atkins, P.; de Paula, J. *Atkins Physical Chemistry*; University Press: Oxford, UK, 2014.
43. O'Leary, D. Nuclear Magnetic Resonance Relaxation by the Antisymmetric Component of the Chemical Shift Tensor: A Longer Transverse Than Longitudinal Relaxation Time, and Intrinsic Deuterium Isotope Effects in Methane, The Conformational Preference of Deuterium and Tritium in Cyclohexane, and a Tritium NMR Method to Assign the Configuration of a Stereogenic (Chiral) Methyl Group. Ph.D. Thesis, University of California, Los Angeles, CA, USA, 1991.
44. Bengs, C.; Levitt, M.H. SpinDynamica: Symbolic and numerical magnetic resonance in a Mathematica environment. *Magn. Reson. Chem.* **2018**, *56*, 374–414. [CrossRef]
45. Erxleben, N.D.; Kedziora, G.S.; Urban, J.J. Anomeric effects in fluoro and trifluoromethyl piperidines: a computational study of conformational preferences and hydration. *Theor. Chem. Acc.* **2014**, *133*, 1491. [CrossRef]
46. Corey, E.; Rohde, J.J. The application of the formyl CH–O hydrogen bond postulate to the understanding of enantioselective reactions involving chiral boron lewis acids and aldehydes. *Tetrahedron Lett.* **1997**, *38*, 37–40. [CrossRef]
47. Cannizzaro, C.E.; Houk, K.N. Magnitudes and Chemical Consequences of $R_3N^+$-C-H···O=C Hydrogen Bonding. *J. Am. Chem. Soc.* **2002**, *124*, 7163–7169. [CrossRef] [PubMed]
48. Scheiner, S. Weak H-bonds. Comparisons of CH···O to NH···O in proteins and PH···N to direct P···N interactions. *Phys. Chem. Chem. Phys.* **2011**, *13*, 13860–13872. [CrossRef]
49. Sandoval-Lira, J.; Fuentes, L.; Quintero, L.; Höpfl, H.; Hernández-Pérez, J.M.; Terán, J.L.; Sartillo-Piscil, F. The Stabilizing Role of the Intramolecular C–H···O Hydrogen Bond in Cyclic Amides Derived From α-Methylbenzylamine. *J. Org. Chem.* **2015**, *80*, 4481–4490. [CrossRef]
50. Kryachko, E.; Scheiner, S. CH···F Hydrogen Bonds. Dimers of Fluoromethanes. *J. Phys. Chem. A* **2004**, *108*, 2527–2535. [CrossRef]
51. Jain, R.; Bally, T.; Rablen, P.R. Calculating Accurate Proton Chemical Shifts of Organic Molecules with Density Functional Methods and Modest Basis Sets. *J. Org. Chem.* **2009**, *74*, 4017–4023. [CrossRef]
52. Bally, T.; Rablen, P.R. Quantum-Chemical Simulation of $^1$H NMR Spectra. 2. Comparison of DFT-Based Procedures for Computing Proton–Proton Coupling Constants in Organic Molecules. *J. Org. Chem.* **2011**, *76*, 4818–4830. [CrossRef]
53. Meier, B.; Dumez, J.N.; Stevanato, G.; Hill-Cousins, J.T.; Roy, S.S.; Håkansson, P.; Mamone, S.; Brown, R.C.D.; Pileio, G.; Levitt, M.H. Long-Lived Nuclear Spin States in Methyl Groups and Quantum-Rotor-Induced Polarization. *J. Am. Chem. Soc.* **2013**, *135*, 18746–18749. [CrossRef]
54. Dumez, J.N.; Håkansson, P.; Mamone, S.; Meier, B.; Stevanato, G.; Hill-Cousins, J.T.; Roy, S.S.; Brown, R.C.D.; Pileio, G.; Levitt, M.H. Theory of long-lived nuclear spin states in methyl groups and quantum-rotor induced polarisation. *J. Chem. Phys.* **2015**, *142*, 044506. [CrossRef] [PubMed]

55. Roy, S.S.; Dumez, J.N.; Stevanato, G.; Meier, B.; Hill-Cousins, J.T.; Brown, R.C.; Pileio, G.; Levitt, M.H. Enhancement of quantum rotor NMR signals by frequency-selective pulses. *J. Magn. Reson.* **2015**, *250*, 25–28. [CrossRef]
56. Dumez, J.N.; Vuichoud, B.; Mammoli, D.; Bornet, A.; Pinon, A.C.; Stevanato, G.; Meier, B.; Bodenhausen, G.; Jannin, S.; Levitt, M.H. Dynamic Nuclear Polarization of Long-Lived Nuclear Spin States in Methyl Groups. *J. Phys. Chem. Lett.* **2017**, *8*, 3549–3555. [CrossRef]